The Canadian Mineralogist
Vol. 36, pp. 1225-1235 (1998)

DISTINCTION OF JAROSITE-GROUP COMPOUNDS BY RAMAN SPECTROSCOPY

KEIKO SASAKI[1], OSAMU TANAIKE and HIDETAKA KONNO

Graduate School of Engineering, Hokkaido University, Sapporo, 060, Japan

Abstract

Raman spectra (200–1300 cm^{-1}) were measured for synthesized jarosite-group compounds [$M Fe_3(SO_4)_2(OH)_6$, $M^+ = K^+$, NH_4^+, Na^+, Ag^+, and $½Pb^{2+}$). The Raman spectra of jarosite-group compounds are characterized by a tendency for the wavenumbers assigned to two vibrational modes of SO_4^{2-}, $\nu_1(SO_4^{2-})$ and $\nu_3(SO_4^{2-})$, and three vibrational modes of Fe–O bonds, to decrease with increase in the *c* unit-cell parameter. The wavenumbers assigned to the $\nu_2(SO_4^{2-})$ and $\nu_4(SO_4^{2-})$ vibrational modes are independent of the value of *c*. For plumbojarosite, the peaks corresponding to the $\nu_1(SO_4^{2-})$ and $\nu_3(SO_4^{2-})$ vibrational modes are broad owing to two overlapping peaks assigned to two types of sulfate groups, SO_4^{2-} ions adjacent and not adjacent to Pb^{2+} ions. Raman spectra can serve to identify the specific type of jarosite-group compound in poorly crystalline or low-concentration geochemical samples.

Keywords: jarosite-group compounds, Raman spectra, monovalent cations, vibrational modes, sulfate, unit-cell parameters.

Sommaire

Nous avons mesuré les spectres de Raman (200–1300 cm^{-1}) d'échantillons synthétiques de composés du groupe de la jarosite [$M Fe_3(SO_4)_2(OH)_6$, $M^+ = K^+$, NH_4^+, Na^+, Ag^+, et $½Pb^{2+}$). Dans ces spectres, la fréquence des vibrations attribuées aux deux modes des groupes SO_4^{2-}, $\nu_1(SO_4^{2-})$ et $\nu_3(SO_4^{2-})$, et des trois modes de vibration associés aux liaisons Fe–O, diminue à mesure qu'augmente le paramètre réticulaire *c*. Les fréquences attribuées au modes de vibration $\nu_2(SO_4^{2-})$ et $\nu_4(SO_4^{2-})$, en revanche, semblent indépendantes de la valeur de *c*. Dans le cas de la plumbojarosite, les pics correspondant aux modes $\nu_1(SO_4^{2-})$ et $\nu_3(SO_4^{2-})$ sont flous à cause de la présence de deux pics qui se chevauchent, attribuables à deux sortes de groupes SO_4^{2-}, adjacents ou non à l'ion Pb^{2+}. Les spectres de Raman peuvent servir pour identifier un membre particulier du groupe de la jarosite dans des échantillons géochimiques à faible cristallinité, où il pourrait être en faible concentration.

(Traduit par la Rédaction)

Mots-clés: composés du groupe de la jarosite, spectres de Raman, cations monovalents, modes de vibration, sulfate, paramètres réticulaires.

Introduction

Jarosite-group compounds [$M Fe_3(SO_4)_2(OH)_6$, where *M* is a monovalent or divalent cation, and *n* is 1 or $^1/_2$] are known to occur in acidic and sulfate-rich environments such as acid mine-drainage (Nordstrom 1982, Taylor *et al.* 1984, Alpers *et al.* 1994, Bigham 1994). Jarosite ($M^+ = K^+$), natrojarosite ($M^+ = Na^+$), ammoniojarosite ($M^+ = NH^{4+}$), argentojarosite ($M^+ = Ag^+$), and plumbojarosite ($M^+ = {}^1/_2\ Pb^{2+}$) are generally distinguished by their X-ray diffraction (XRD) patterns. However, the detection limit of XRD analysis is high; trace amounts of jarosite in geochemical samples and poorly crystalline material cannot be detected by XRD (Sasaki *et al.* 1993). Samples containing jarosite-group minerals are important as geochemical indicators; the presence of jarosite in geochemical samples provides evidence that sampling sites are strongly acidic (Filipek *et al.* 1987), and so it is important to establish sensitive methods to detect and distinguish jarosite-group phases. Vibrational spectroscopy has been applied to the analysis of various minerals, and infrared spectra of jarosite-group compounds have been reported by several investigators (Adler & Kerr 1965, Lazaroff *et al.* 1982, Serna *et al.* 1986, Sasaki *et al.* 1993). Infrared spectroscopy has been used to distinguish sulfate minerals with different symmetries, but not jarosite-group minerals with similar symmetry. Raman spectra of jarosite-group

[1] *Present address*: Laboratory of Environmental Science, Otaru University of Commerce, Otaru, 047-8501, Japan. *E-mail address*: keikos@res.otaru-uc.ac.jp

compounds have not been fully reported, though the Raman spectrum for natrojarosite has been reported and compared with that for natro-alunite (Serna *et al.* 1986).

The present work discusses and compares Raman spectra for jarosite [$KFe_3(SO_4)_2(OH)_6$], ammoniojarosite [$NH_4Fe_3(SO_4)_2(OH)_6$], natrojarosite [$NaFe_3(SO_4)_2(OH)_6$], argentojarosite [$AgFe_3(SO_4)_2(OH)_6$], and plumbojarosite [$Pb_{½}Fe_3(SO_4)_2(OH)_6$] with Fourier transform infrared spectra (FTIR). Further, vibrational spectroscopy was applied to the identification of secondary minerals by microbially mediated dissolution of pyrite.

Materials and Methods

Standard jarosite-group compounds

The jarosite-group compounds listed above were synthesized in an autoclave as verified by their XRD pattern and elemental composition (Dutrizac & Kaiman 1976, Sasaki *et al.* 1995). The structure and crystallographic parameters are shown in Figure 1 and Table 1. The M^+ ions are present in 12-coordination between six O and six OH. The Fe^{3+} ions are in 6-coordination to four OH and two O. The *c* unit-cell parameter tends to increase with increasing ionic radius of M^+, though there are other factors also affecting it.

Microbially mediated dissolution of pyrite

A 3.75-g sample of ground and pretreated pyrite (FeS_2, 0.40 $m^2\ g^{-1}$) (Sasaki *et al.* 1996) was added to a porous-plugged 500-cm^3 Erlenmeyer flask with 150 cm^3 of the 9K medium of Silverman (15 mmol dm^{-3} $(NH_4)_2SO_4$, 2.0 mmol dm^{-3} $MgSO_4 \cdot 7H_2O$, 1.3 mmol dm^{-3} KCl, 5.7 mmol dm^{-3} K_2HPO_4, 0.061 mmol dm^{-3} $Ca(NO_3)_2$, and 160 mmol dm^{-3} $FeSO_4 \cdot 7H_2O$ as an energy source, pH 2.0) (Silverman & Lundgren 1959): two experiments were carried out, one by inoculation with 4.20×10^9 cells of the iron-oxidizing bacterium, *Thiobacillus ferrooxidans* (HUTY 8906) (Sasaki *et al.* 1993), and the other sterile (without bacteria). The flasks were installed in a rotary shaking culture-apparatus at 30°C and incubated for 5 weeks. At intervals, one cm^3 of supernatant liquid was pipetted off and filtered through a 0.20-μm-pore membrane filter for determination of dissolved Fe, S, and K species in the filtrate by inductively coupled plasma – atomic emission spectrometry (ICP–AES: SEIKO Co. Ltd. SPS 1200) and measurements of pH and redox potential, E. After 5 weeks, the residues were separated by filtration using a Whatman 41 filter and vacuum-dried for XRD, FTIR, and Raman spectroscopic analysis.

TABLE 1. CRYSTALLOGRAPHIC PARAMETERS OF JAROSITE-GROUP COMPOUNDS [$MFe_3(SO_4)_2(OH)_6$]

Compound	Ionic radius* of M^+	Unit-cell parameters *a*	*c*	JCPDS No.
jarosite	1.33 Å	7.29 Å	17.22 Å	10-443
ammoniojarosite	1.48	7.327	17.50	26-1014
natrojarosite	0.95	7.34	16.72	11-302
argentojarosite	1.26	7.35	16.58	25-1327
plumbojarosite	1.21	7.335	33.85	33-759

* ionic radius (Shannon & Prewitt 1969).

Raman spectroscopy

For Raman spectroscopy, excitation was accomplished by light of a single wavelength (514.5 nm) from an Ar ion laser. The incident power was about 38 mW at the sample point. The Raman scattered light was detected by a laser Raman spectrometer (JASCO NRS 2000). The samples were diluted to 5 wt% with KBr powder, and 0.30 g of the mixture was compressed to form a disk 10 mm in diameter. A rotating apparatus was used for the measurement of the disk to avoid heat-

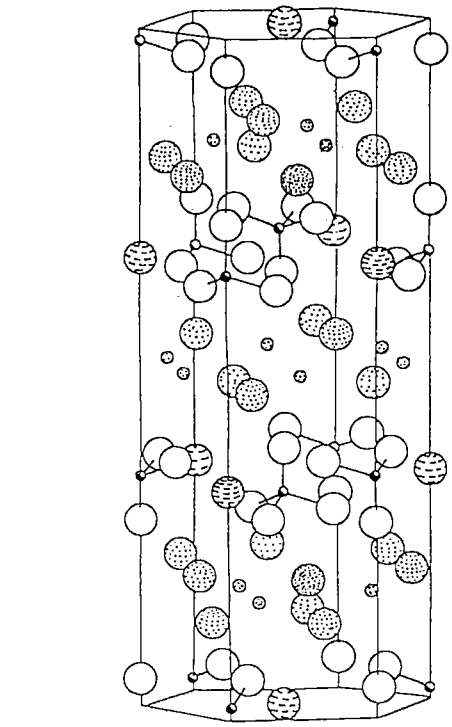

FIG. 1. The structure of jarosite-group compounds, $M_3Fe_9(SO_4)_6(OH)_{18}$ (Brophy *et al.* 1962).

ing effects of the laser beam. The laser light was standardized with silicon, using a band maximum at 520 cm^{-1}, polarized parallel to the plane of incidence, and the angle of incidence was 80°. The Raman scattered light was collected in the plane of incidence in the direction normal to the incident laser light. The Raman spectra were obtained from 200 to 1300 cm^{-1} after three accumulations using 10- and 60-second integration times for the standard jarosite-group compounds and samples containing pyrite, respectively.

FTIR

Infrared spectra were recorded with an FTIR spectrometer (JASCO VALOR III) using diffuse reflectance infrared Fourier transform spectroscopy (DRIFTS) with 0.6 (w/w) % of sample in KBr, under the following conditions: accumulation, 16 times; resolution, 4 cm^{-1}; detector, TGS; range of wavenumbers, 400–4000 cm^{-1} (Sasaki *et al.* 1995).

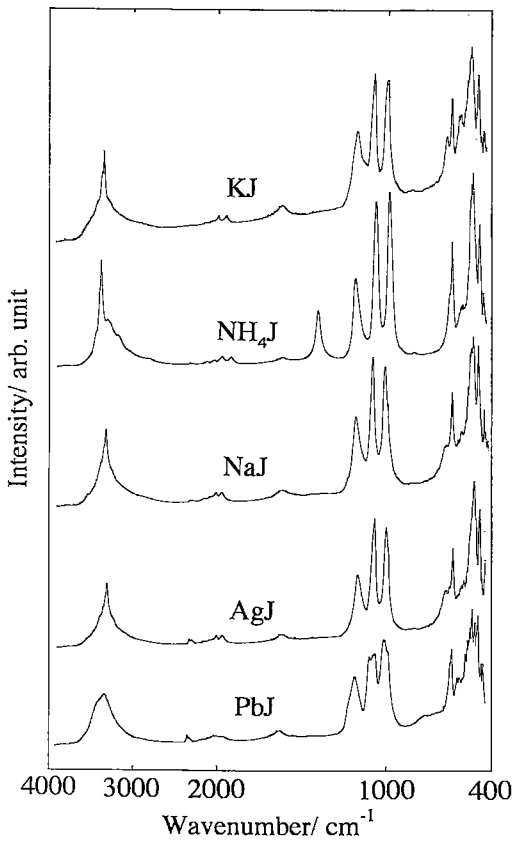

FIG. 2. FTIR spectra for jarosite (KJ), ammoniojarosite (NH_4J), natrojarosite (NaJ), argentojarosite (AgJ), and plumbojarosite (PbJ).

XRD

The powder X-ray diffraction patterns of samples were collected with a JEOL JDX–3500 diffractometer with a monochromator under the following conditions: Cu*K*α radiation, 30 kV, 200 mA; step-scanning method; time constant, 0.5 second.

RESULTS

Standard jarosite-group compounds

Figure 2 shows FTIR spectra from 400 to 4000 cm^{-1} for jarosite, ammoniojarosite, natrojarosite, argentojarosite, and plumbojarosite. Three spectra are very similar, whereas ammoniojarosite and plumbojarosite show some differences. All spectra have one group of peaks at 3350–3420 cm^{-1} assigned to the stretching vibration mode of O–H, and three strong peaks at 1000–1200 cm^{-1} assigned to the vibration modes of $\nu_3(SO_4^{2-})$ (at two higher wavenumbers) and $\nu_1(SO_4^{2-})$ (at the lowest wavenumber). Ammoniojarosite has an additional peak at 1420 cm^{-1} assigned to the ν_4 bending vibration mode of NH^{4+}. Plumbojarosite has three broad and divided peaks around 1000–1200 cm^{-1}. All peak assignments are summarized in Table 2.

Raman spectra from 200 to 700 cm^{-1} and from 900 to 1300 cm^{-1} for jarosite, ammoniojarosite, natrojarosite, argentojarosite, and plumbojarosite are shown in Figures 3 and 4. No peaks were observed between 700 and 900 cm^{-1} in any spectrum. Assignments are listed in Table 2, together with IR-assignments. As shown in Figure 3 and Table 2, there are shoulder bands around 448–455 cm^{-1} assigned to the vibrational mode of $\nu_2(SO_4^{2-})$, and sharp bands around 622–625 cm^{-1} assigned to the vibrational mode of $\nu_4(SO_4^{2-})$ in jarosite-group compounds. There are no clear differences among the wavenumber-values at two bands of $\nu_2(SO_4^{2-})$ and $\nu_4(SO_4^{2-})$ in the five spectra, though there are different patterns at wavenumbers smaller than 440 cm^{-1} assigned to the vibrational modes of Fe–O bonding. From 900 to 1300 cm^{-1} (Fig. 4), there are bands around 1000–1015 cm^{-1} and around 1090–1115 cm^{-1}, assigned to the vibrational modes of $\nu_1(SO_4^{2-})$ and $\nu_3(SO_4^{2-})$, respectively. There are peak shifts depending on the M^+ ions involved. Weak bands around 1153–1169 cm^{-1} are also observed in all spectra and assigned to the vibrational mode of $\nu_3(SO_4^{2-})$. For plumbojarosite, there are three broad bands around 990–1030 cm^{-1} [$\nu_1(SO_4^{2-})$], around 1080–1120 cm^{-1} [$\nu_3(SO_4^{2-})$], and around 1160–1180 cm^{-1} [$\nu_3(SO_4^{2-})$] apparently due to overlapping multiple components.

Residue after microbially mediated dissolution of pyrite

Figure 5 shows XRD patterns of pyrite samples after 5 weeks of dissolution with and without *T.*

ferrooxidans. There are two groups of peaks assigned to pyrite (JCPDS 6–0710) and jarosite-group minerals (jarosite or ammoniojarosite, or both) in the presence of bacteria, whereas there is a single group of peaks assigned to pyrite in the absence of bacteria. This indicates that secondary minerals were formed during the microbially mediated dissolution of pyrite. However, it is difficult to identify the secondary minerals by XRD alone, since *d*-values of jarosite (JCPDS 10–443) are very similar to those of ammoniojarosite (JCPDS 26–1014).

The FTIR spectra of the pyrite samples after the 5-week dissolution are shown in Figure 6. There are three peaks around 1000–1200 cm^{-1} in both spectra. It is not clear whether there are differences in the

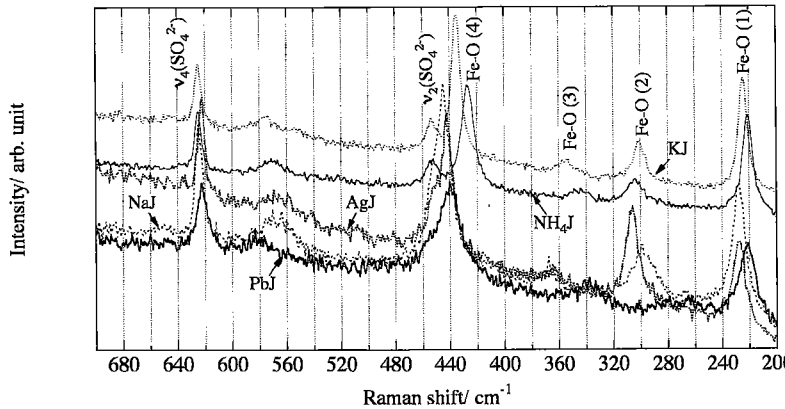

FIG. 3. Raman spectra between 200 and 700 cm^{-1} for jarosite (KJ), ammoniojarosite (NH_4J), natrojarosite (NaJ), argentojarosite (AgJ), and plumbojarosite (PbJ).

TABLE 2. ASSIGNMENTS OF INFRARED (IR) AND RAMAN WAVENUMBERS IN JAROSITE-GROUP COMPOUNDS [$MFe_3(SO_4)_2(OH)_6$]

Wavenumbers/ cm^{-1}										Assignments
$M^+ = K^+$		$M^+ = NH_4^+$		$M^+ = Na^+$		$M^+ = Ag^+$		$M^+ = 1/2\ Pb^{2+}$		
IR	Raman	IR	Raman	IR	Raman	IR	Raman	IR	Raman	
3390sp		3420sp								ν_{OH}
3365				3365sp		3350sp		3350		ν_{OH}
-		1420sp		-		-		-		N-H
1190	1153.33	1200	1160.58	1200	1154.24w	1190	1160.58w	1195	1168.72w	$\nu_3(SO_4^{2-})$
1088s	1102.63s	1080s	1091.77s	1098s	1112.59	1092s	1107.16	1110*	1120*	$\nu_3(SO_4^{2-})$
								1080*	1108*	$\nu_3(SO_4^{2-})$
1028s		1002s		1027s		1021s		1021		δ(OH)
1010	1006.67	1000	1005.76	1012sh	1012.10	1010sh	1012.10	1016*	1015*	$\nu_1(SO_4^{2-})$
								1000*	1002*	$\nu_1(SO_4^{2-})$
660		655		675		670		668		$\nu_4(SO_4^{2-})$
630sp	624.61sp	635sp	624.61sp	630sp	624.61sp	630sp	622.80sp	622sp	622.80sp	$\nu_4(SO_4^{2-})$
580	576.63w	580	571.19w	570	570.29w	567	573.91w	580	582.96w	γ(OH)
520		508		512		508		504		O-Fe
478		472		480						O-Fe
448	453.50	450	454.40	448	450.78sh	440	448.97sh	440	451.69sh	$\nu_2(SO_4^{2-})$
	434.49s		427.24s	406	444.44s		441.73s		439.92s	O-Fe
	357.53w		348.48w		367.49w		362.96w		341.24w	O-Fe
	301.40		303.21		298.68		305.93sp		-	O-Fe
	223.54s		220.82s		227.16		228.07		220.82	O-Fe

s: strong; w: weak; sh: shoulder; b: broad; sp: sharp; *: separated peak.

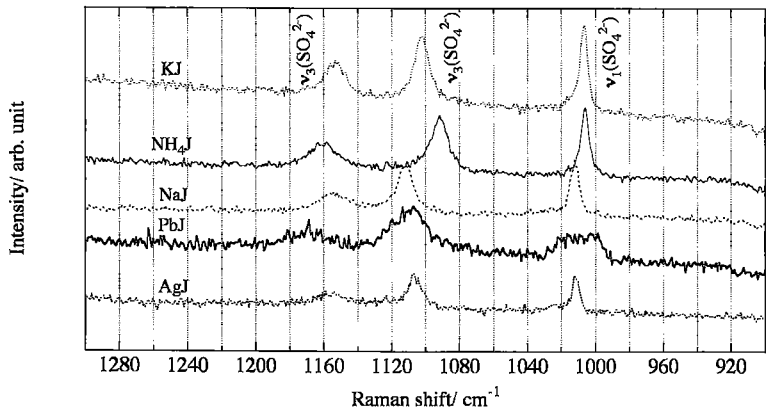

FIG. 4. Raman spectra between 900 and 1300 cm^{-1} for jarosite (KJ), ammoniojarosite (NH_4J), natrojarosite (NaJ), argentojarosite (AgJ), and plumbojarosite (PbJ).

TABLE 3. CORRELATION COEFFICIENTS OF LINEAR RELATIONSHIP BETWEEN VIBRATIONAL WAVENUMBERS AND CELL PARAMETER *c* IN VIBRATIONAL MODES $\nu_1(SO_4^{2-})$ AND $\nu_3(SO_4^{2-})$ IN RAMAN AND IR SPECTRA OF JAROSITE-GROUP COMPOUNDS*

	Raman	IR
$\nu_1(SO_4^{2-})$	0.9644	0.8486
$\nu_3(SO_4^{2-})$	0.9832	0.8844

* Figure 9.

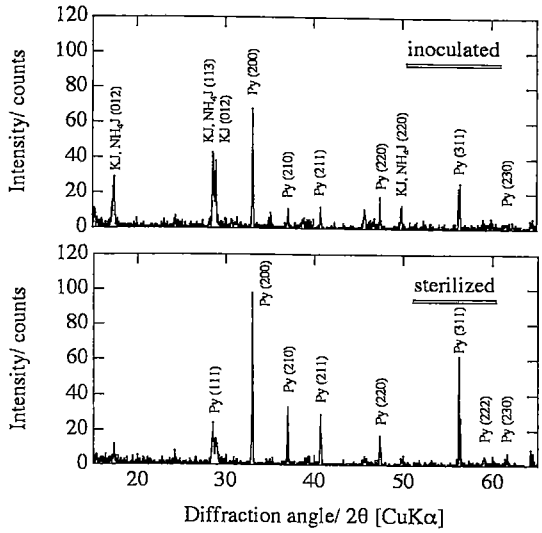

FIG. 5. XRD patterns of pyrite after five weeks of dissolution in the presence (top) and absence (bottom) of *Thiobacillus ferrooxidans*. Py: pyrite; KJ: jarosite; NH_4J: ammoniojarosite.

wavenumbers of the two spectra in the 1000–1200 cm^{-1} region, as the peaks in a spectrum of the sterile sample are broad. However, there is a peak at 1422 cm^{-1} assigned to the $\nu_4(NH_4^+)$ in the inoculated sample, which is absent in the spectrum of the sterilized sample. There are no peaks assigned to the vibrational modes of the Fe–S bond at 400–4000 cm^{-1} in the IR spectrum (Sasaki *et al.* 1996).

The Raman spectra show seven bands (Fig. 7) assigned to the vibrational modes of Fe–O and S–O bonding in jarosite-group compounds, in addition to two bands at 353 and 387 cm^{-1} assigned to the vibrational modes of Fe–S bonding in pyrite (FeS_2) and a band at 470 cm^{-1} assigned to the stretching modes of S–S in elemental sulfur (Li *et al.* 1992). The Raman wavenumbers of jarosite-group compounds are listed in Table 3. The bands around 340–360 cm^{-1} assigned to Fe–O bonds are hidden by strong bands assigned to Fe–S bonds in FeS_2. Figure 7 and Table 3 show that there are four clear peak-shifts between the two spectra (marked by *): around 300 cm^{-1} (assigned to the Fe–O vibrational mode), 420–440 cm^{-1} (assigned to the Fe–O vibrational mode), 1090–1100 cm^{-1} [assigned to the $\nu_3(SO_4^{2-})$ vibrational mode], and 1150–1160 cm^{-1} [assigned to the $\nu_3(SO_4^{2-})$ vibrational mode].

Less than one week was required to completely consume the dissolved K^+ ions in the inoculated medium, whereas more than five weeks were required in the sterile medium. Details of the solution analysis were reported elsewhere (Sasaki 1997).

DISCUSSION

Standard spectra for jarosite-group compounds

The vibrational modes of $\nu_1(SO_4^{2-})$, $\nu_2(SO_4^{2-})$, $\nu_3(SO_4^{2-})$ and $\nu_4(SO_4^{2-})$ are generally illustrated as in Figure 8: ν_1 and ν_3 are the stretching modes, and ν_2 and

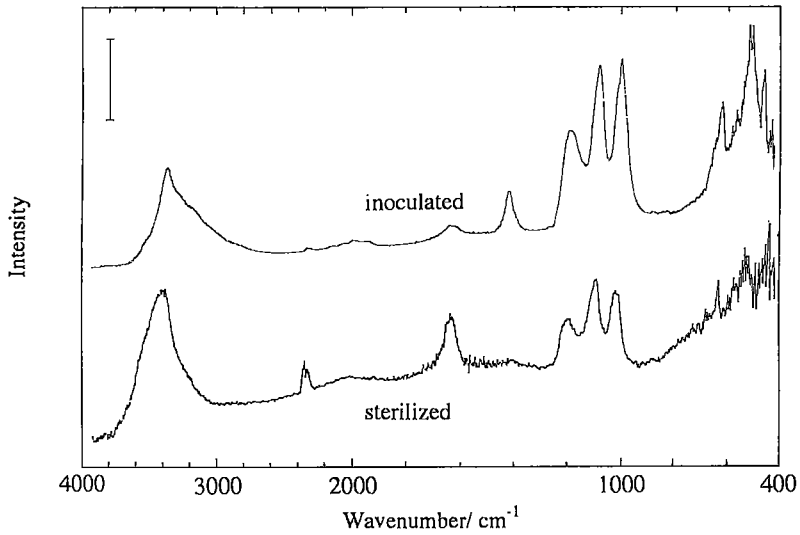

FIG. 6. FTIR spectra of pyrite after five weeks of dissolution in the presence (top) and absence (bottom) of *Thiobacillus ferrooxidans*. A vertical bar indicates 2 and 0.2 Kubelka–Munk units for the inoculated and sterile samples.

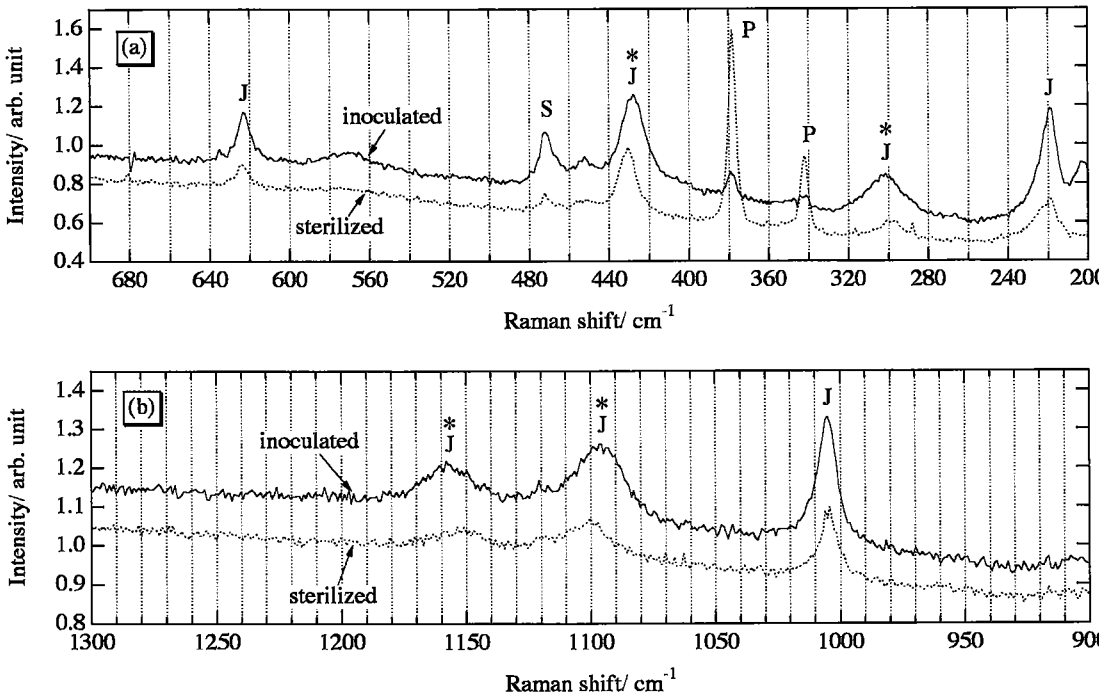

FIG. 7. Raman spectra at 200–700 cm^{-1} (a) and 900–1300 cm^{-1} (b) of pyrite after five weeks of dissolution in the presence and absence of *Thiobacillus ferrooxidans*. P: pyrite, S: elemental sulfur, J: jarosite-group compounds.

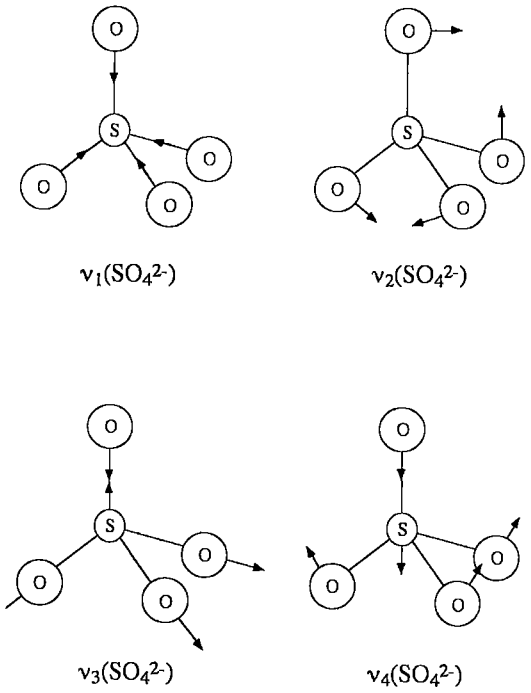

FIG. 8. The $\nu_1(SO_4^{2-})$, $\nu_2(SO_4^{2-})$, $\nu_3(SO_4^{2-})$ and $\nu_4(SO_4^{2-})$ vibrational modes.

ν_4 are the bending modes. In SO_4 tetrahedra (*Td*), all four vibrations are Raman-active, whereas only $\nu_3(SO_4^{2-})$ and $\nu_4(SO_4^{2-})$ are infrared-active (F_2) (Gadsden 1975). However, the SO_4^{2-} ions in jarosite-group compounds have C_3v site symmetry (Serna *et al.* 1986). This lowering of symmetry splits the degenerate vibrations and activates infrared-inactive vibrations; in C_3v site symmetry, $\nu_1(SO_4^{2-})$, $\nu_3(SO_4^{2-})$, and $\nu_4(SO_4^{2-})$ are infrared- and Raman-active (A_1), and $\nu_2(SO_4^{2-})$, $\nu_3(SO_4^{2-})$, and $\nu_4(SO_4^{2-})$ are infrared and Raman active (E). Therefore, as shown in Figures 2–4 and Table 2, the four vibrational modes of $\nu_1(SO_4^{2-})$, $\nu_2(SO_4^{2-})$, $\nu_3(SO_4^{2-})$, and $\nu_4(SO_4^{2-})$ are infrared and Raman active.

As shown in Table 1, the c unit-cell parameter in jarosite-group compounds (except plumbojarosite) tends to increase with increasing ionic radius of the M^+ ions, whereas the a parameter is independent of the ionic radius of M^+ ions. Based on the Raman spectra in Figures 3 and 4, $\nu_1(SO_4^{2-})$, $\nu_2(SO_4^{2-})$, $\nu_3(SO_4^{2-})$, and $\nu_4(SO_4^{2-})$, are plotted against the c parameter (Fig. 9). Note that $\nu_3(SO_4^{2-})$, near 1153–1169 cm^{-1}, was not used because the weakness of the bands leads to a large uncertainty in their exact position, and half the c parameter value was used for plumbojarosite in Figure 9; the wavenumbers of the IR bands are also plotted against the c parameter. The $\nu_1(SO_4^{2-})$ and $\nu_3(SO_4^{2-})$ decrease significantly (approximately linearly) with increases in the c parameter except for plumbojarosite, and $\nu_2(SO_4^{2-})$ and $\nu_4(SO_4^{2-})$ are independent of the c parameter. The peculiarities of plumbojarosite will be discussed later.

It is not difficult to explain why the frequency of the stretching mode depends on c, whereas the frequency of the bending mode is independent of c. Generally, the frequency of vibrations, ν, is expressed by

$$\nu = (1/2\pi)\,(k/\mu)^{1/2}, \quad (1)$$

where μ is the reduced mass, and k is the force constant. In jarosite-group compounds, the cell parameter c increases with an increase of ionic radius of the M^+ ions, which also leads to a decrease in the polarization of the S–O bonds, since M^+ ions are in the same layer as the (SO_4^{2-}) ions (Fig. 1). This decrease in polarization results in a decrease of k for the stretching modes $\nu_1(SO_4^{2-})$ and $\nu_3(SO_4^{2-})$, whereas it does not affect k for the bending modes $\nu_2(SO_4^{2-})$ and $\nu_4(SO_4^{2-})$. The reduced mass, μ, is independent of vibrational mode. Therefore, $\nu_1(SO_4^{2-})$ and $\nu_3(SO_4^{2-})$ will decrease with increase of the cell parameter c, whereas $\nu_2(SO_4^{2-})$ and $\nu_4(SO_4^{2-})$ will be independent of c.

As shown in Figure 9, $\nu_1(SO_4^{2-})$ and $\nu_3(SO_4^{2-})$ decrease approximately linearly with increases in the c parameter (in the order argentojarosite < natrojarosite < jarosite < ammoniojarosite) brought about by incorporation of cations of different ionic radius. The correlation between the $\nu_1(SO_4^{2-})$ and $\nu_3(SO_4^{2-})$ wavenumbers and the c parameter is better for Raman wavenumbers (solid lines) than for IR wavenumbers (broken lines), as shown in Table 3 and Figure 9. For the vibrational modes of S–O in jarosite compounds, Raman spectra at high wavenumbers (900–1300 cm^{-1}) were useful to distinguish the jarosite-group compounds from each other, since the $\nu_1(SO_4^{2-})$ and $\nu_3(SO_4^{2-})$ bands appear there.

At low wavenumbers (200–700 cm^{-1}), there are four Raman bands assigned to the vibrations of Fe–O bonds in the jarosite-group compounds other than plumbojarosite (Fig. 3). The relationship between the four Raman shifts at 220–228 (1), 298–306 (2), 341–368 (3), and 427–445 (4) cm^{-1}, and the c parameter in jarosite-group compounds is shown in Figure 10. In the spectrum for plumbojarosite (Fig. 3), there are only three Raman bands assigned to the vibrations of Fe–O bonds: the two bands around 298–306 (2) and 341–368 (3) cm^{-1} come closer together to give a single band around 340 cm^{-1}. The three Raman shifts around 220–228 (1), 341–368 (3), and 427–445 (4) cm^{-1} tend to decrease with increasing c parameter, whereas there is no simple relationship between Raman shifts around 298–306 (2) cm^{-1} and the c parameter. As shown in Figure 1, increases in the c parameter of jarosite-group compounds increase the distance between Fe and O atoms, resulting in decreases in Raman shifts of the Fe–O vibrational modes according to equation (1). Jarosite-

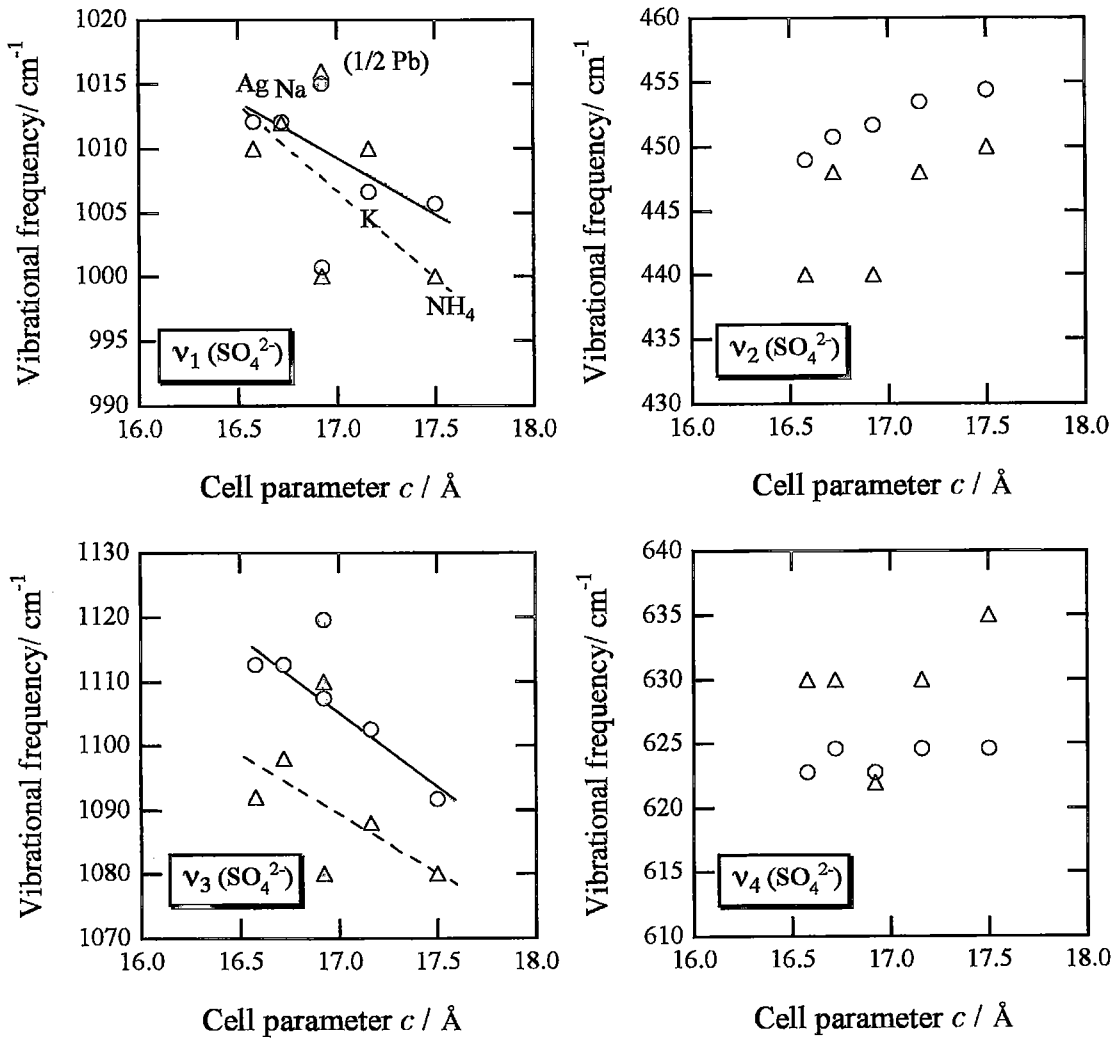

FIG. 9. Relationship between Raman shifts of $\nu_1(SO_4^{2-})$, $\nu_2(SO_4^{2-})$, $\nu_3(SO_4^{2-})$ and $\nu_4(SO_4^{2-})$, and the cell parameter c in jarosite-group compounds. Symbols: ○ and ●: Raman wavenumbers; △ and ▲: IR wavenumbers. Solid symbols indicate separated peaks in the original spectra of the plumbojarosite. _____ Raman, _ _ _ _ _ infrared least-squares hits.

group compounds can be identified with improved accuracy by using both the Raman spectra at high wavenumbers (900–1300 cm^{-1}) and those at low wavenumbers (200–700 cm^{-1}). There is no useful information on Fe–O bonding in the IR spectra in the interval 400–4000 cm^{-1}.

The unit structure of plumbojarosite has a c parameter approximately double that of jarosite-group compounds containing monovalent cations, as shown in Table 1, and Pb^{2+} ions occupy every other M^+ site. Therefore, there are two types of SO_4^{2-} in a unit structure of plumbojarosite: one is SO_4^{2-} adjacent to Pb^{2+} ions, and the other is SO_4^{2-} adjacent to vacant sites. It is assumed that the $\nu_1(SO_4^{2-})$ and $\nu_3(SO_4^{2-})$ values assigned to S–O bonds in sulfate adjacent to Pb^{2+} ions are smaller than those in sulfate not adjacent to Pb^{2+} ions. A plateau peak around 1000–1200 cm^{-1} assigned to the vibrational mode of $\nu_1(SO_4^{2-})$ and a broad peak around 1105–1115 cm^{-1} assigned to the vibrational mode of $\nu_3(SO_4^{2-})$ in plumbojarosite were separated by computer fitting using the Gaussian–Lorentzian mixed functions. The former was divided into two components with peaks at 1000.7 and 1015.1 cm^{-1}, and the latter, into two components with peaks at 1107.5 and 1119.6 cm^{-1}.

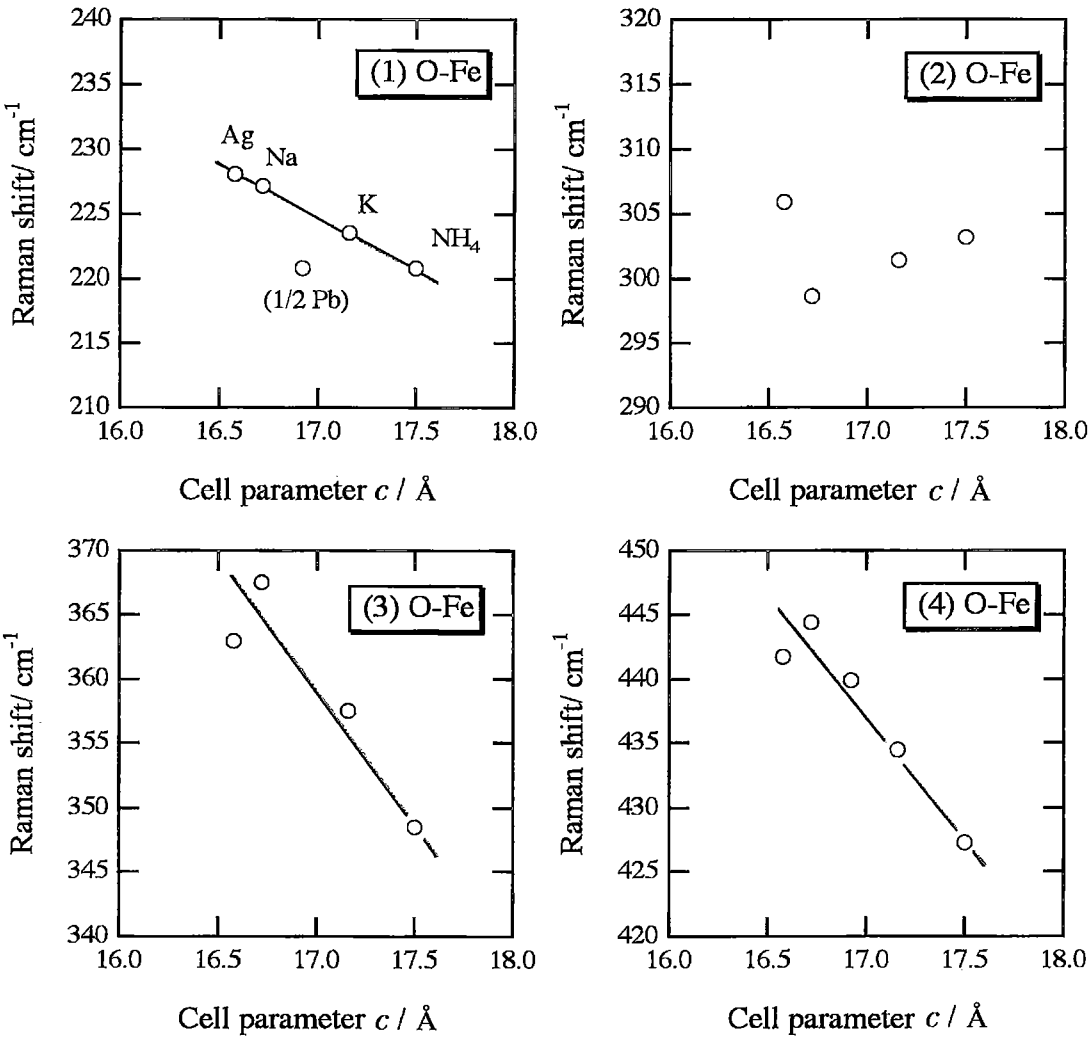

FIG. 10. Relationship between four Raman shifts assigned to the vibrational modes of Fe–O bonds, and the *c* unit-cell parameter in jarosite-group compounds.

The separated $\nu_1(SO_4^{2-})$ and $\nu_3(SO_4^{2-})$ values are shown by solid circles in Figure 9. Also, IR-wavenumbers of $\nu_1(SO_4^{2-})$ and $\nu_3(SO_4^{2-})$ for plumbojarosite were deconvoluted similarly, and are indicated by solid triangles in Figure 9. On the other hand, two bands assigned to $\nu_2(SO_4^{2-})$ and $\nu_4(SO_4^{2-})$ in a spectrum of plumbojarosite in Figure 3 are not split in this way, though the $\nu_2(SO_4^{2-})$ band has a shoulder near a strong band due to Fe–O bond vibrations. Presumably the vibrational modes $\nu_2(SO_4^{2-})$ and $\nu_4(SO_4^{2-})$ are much less independent on the nature of the M^+ cation (Fig. 8). Similar effects were also observed in the IR spectra (Fig. 2, Table 2).

Identification of secondary minerals in microbially mediated dissolution of pyrite

As described in the previous section, it was impossible to distinguish the kinds of jarosite-group compounds by XRD alone, though secondary minerals in inoculated samples were identified as containing such compounds. The peak at 1422 cm^{-1} in the FTIR spectrum suggests that it contains ammoniojarosite. The Raman spectrum (Fig. 7, Table 4) shows that it is predominantly ammoniojarosite, on the basis of the details of the standard spectrum of jarosite-group compounds as discussed above. It is assumed that dissolved NH_4^+ and K^+ ions in

TABLE 4. RAMAN WAVENUMBERS OF SECONDARY MINERALS IN THE MICROBIALLY MEDIATED DISSOLUTION OF PYRITE

Samples	Wavenumbers/ cm^{-1}							
	Fe-O (1)	Fe-O (2)	Fe-O (4)	$\nu_2(SO_4^{2-})$	$\nu_4(SO_4^{2-})$	$\nu_1(SO_4^{2-})$	$\nu_3(SO_4^{2-})$	$\nu_3(SO_4^{2-})$
inoculated	219.0	*303.1	*428.0	453.0	624.0	1006.1	*1095.7	*1160.7
sterile	219.0	*299.4	*431.6	452.0	624.3	1005.2	*1100.1	*1150.7

* wavenumbers which characterize the changes.

the 9K medium were involved in crystallization of jarosite-group compounds, and that the rapid decrease in the concentration of the K^+ ion in the medium resulted in the formation of only small amounts of jarosite.

For the sterile sample, secondary minerals were not detected in an XRD pattern. Only the FTIR spectrum indicates that jarosite-group compounds formed, though the intensities of signals are weak and the nature of the compounds could not be specified. However, the Raman spectrum shows that it is very similar to jarosite but not to ammoniojarosite (Tables 2, 4). The reason why various types of jarosite-group compounds were predominantly formed in the inoculated and sterile samples was discussed in detail elsewhere (Sasaki 1997).

Our findings indicate that it is possible in practice to apply Raman spectroscopy to the identification of specific secondary jarosite-group minerals formed during the microbially mediated dissolution of pyrite.

Conclusions

Jarosite-group compounds can be distinguished by Raman spectroscopy. The frequencies (Raman shifts) assigned to $\nu_1(SO_4^{2-})$ and $\nu_3(SO_4^{2-})$, and three vibrational modes of Fe–O bonds decrease significantly with increases in the *c* unit-cell parameter. Two vibrational modes, $\nu_2(SO_4^{2-})$ and $\nu_4(SO_4^{2-})$, are independent of the *c* parameter. For plumbojarosite, the bands due to $\nu_1(SO_4^{2-})$ and $\nu_3(SO_4^{2-})$ are broadened owing to the mixture of two types of SO_4^{2-}, one with SO_4^{2-} adjacent to Pb^{2+} ions, and one where SO_4^{2-} is not adjacent to Pb^{2+} ions. Jarosite-group compounds formed as secondary phases during the biotic or abiotic dissolution of pyrite were specifically identified by Raman spectroscopy; this could not be accomplished by XRD and FTIR. Raman spectroscopy provided useful information to identify specific jarosite-group minerals in geochemical samples.

Acknowledgements

Appreciation is extended to Dr. J.E. Dutrizac of CANMET (Ottawa), for supplying standard jarosite-group compounds and to the two anonymous referees. This work was supported by Hayashi Memorial Foundation for Female Natural Scientists.

References

Adler, H.H. & Kerr, P.F. (1965): Variations in infrared spectra, molecular symmetry and site symmetry of sulfate minerals. *Am. Mineral.* **50**, 132-147.

Alpers, C.N., Blowes, D.W., Nordstrom, D.K. & Jambor, J.L. (1994): Secondary minerals and acid mine-water chemistry. *In* Environmental Geochemistry of Sulfide Mine-Wastes (J.L. Jambor & D.W. Blowes, eds.). *Mineral. Assoc. Can., Short-Course Vol.* **22**, 247-270.

Bigham, J.M. (1994): Mineralogy of ochre deposits formed by sulfide oxidation. *In* Environmental Geochemistry of Sulfide Mine-Wastes (J.L. Jambor & D.W. Blowes, eds.). *Mineral. Assoc. Can., Short-Course Vol.* **22**, 103-132.

Brophy, G.P., Scott, E.S. & Snellgrove, R.A. (1962): Sulfate studies. II. Solid solution between alunite and jarosite. *Am. Mineral.* **47**, 112-126.

Dutrizac, J. E. & Kaiman, S. (1976): Synthesis and properties of jarosite-type compounds. *Can. Mineral.* **14**, 151-158.

Filipek, L.H., Nordstrom, D.K. & Ficklin, W.H. (1987): Interaction of acid mine drainage with waters and sediments of West Squaw Creek in the West Shasta mining district, California. *Environ. Sci. Technol.* **21**, 388-396.

Gadsden, J.A. (1975): *Infrared Spectra of Minerals and Related Compounds*. Butterworth, London, U.K.

Lazaroff, N., Sighal, W. & Wasserman, A. (1982): Iron oxidation and precipitation of ferric hydroxysulfates by resting *Thiobacillus ferrooxidans* cells. *Appl. Environ. Microbiol.* **43**(4), 924-938.

Li, J., Zhu, X. & Wadsworth, M.E. (1992): *Raman Spectroscopy of Natural and Oxidized Metal Sulfides* (J.P. Hager, ed.). The Mineral & Materials Society (229-244).

Nordstrom, D.K. (1982): Aqueous pyrite oxidation and the consequent formation of secondary iron minerals. *In* Acid Sulfate Weathering (L.R. Hossaer, ed.). Soil Sci. Soc. Am., Madison, Wisconsin (37-63).

Sasaki, K. (1997): Raman study of the microbially mediated dissolution of pyrite by *Thiobacillus ferrooxidans*. *Can. Mineral.* **35**, 999-1008.

_____, TSUNEKAWA, M. & KONNO, H. (1995): Characterization of argentojarosite formed from biological oxidized Fe^{3+} ions. *Can. Mineral.* **33**, 1311-1319.

_____, _____, _____, HIRAJIMA, T. & TAKAMORI, T. (1993): Leaching behavior and surface characterization of pyrite in bacterial leaching with *Thiobacillus ferrooxidans*. *Shigen-to-Sozai* **109**, 29-35 (in Japanese, with English abstr.).

_____, _____, TANAKA, S. & KONNO, H. (1996): Suppression of microbially mediated dissolution of pyrite by originally isolated fulvic acid and the related compounds. *Colloids and Surfaces. A. Physicochemical and Engineering Aspects* **119**, 241-253.

SERNA, C.J., CORTINA, C.P. & GARCIA-RAMOS, J.V. (1986): Infrared and Raman study of alunite – jarosite compounds. *Spectrochimica Acta* **42A**, 729-734.

SHANNON, R.D. & PREWITT, C.T. (1969): Effective ionic radii in oxides and fluorides. *Acta Crystallogr.* **B25**, 925-946.

SILVERMAN, M.P. & LUNDGREN, D.G. (1959): Studies on the chemoautotrophic iron bacterium *Ferrobacillus ferrooxidans*. 1. An improved medium and a harvesting procedure for securing high cell yield. *J. Bacteriol.* **77**, 642-647.

TAYLOR, B.E., WHEELER, M.C. & NORDSTROM, D.K. (1984): Stable isotope geochemistry of acid mine drainage: experimental oxidation of pyrite. *Geochim. Cosmochim. Acta* **48**, 2669-2678.

Received October 20, 1997, revised manuscript accepted October 10, 1998.